The Future of Gas Turbine Technology
8th International Gas Turbine Conference
12-13 October 2016, Brussels, Belgium

Paper ID Number (*25-IGTC16)*

TURBOMACHINERY-BASED ENGINE: CONCURRENT PRODUCTION OF POWER, COOLING AND DESALINATED WATER

Giovanni Cerri[1], Leila Chennaoui[1], Stefano Mazzoni[1], Norbert Buchsbaum[2]
[1]Roma Tre University, Department of Engineering, Rome, Italy
[2]CryoDesalination LLC, Houston TX, USA

Via Vito Volterra, 62 00146 Rome Italy
+39 06 57333251
cerri@uniroma3.it

ABSTRACT
A special turbomachinery-based engine ©GICE has been proposed for the concurrent production of power and cold. The High Temperature Heat injected into the cycle allows an expansion at temperatures lower than the environment temperature.
A ©GICE engine coupled with a novel seawater ©CryoDesalination plant has been investigated to concurrently produce power, pure water and cold suitable for air conditioning.
An ample discussion of results is reported in the paper.

NOMENCLATURE

ADGT	Aero-Derivative Gas Turbine
C	Compressor
CEG	Compressor Expander Group
CETT	Car Engine Turbocharger Technology
CP	Cold Power
c_p	Pressure Specific Heat
c_v	Volume Specific Heat
DB	Data Base
DNI	Direct Normal Irradiation
E	Expander, Efficacy
ER	Ericsson
E&CM	Easy & Cheap Maintenance
GICE	Engine/Cycle Arrangement
HDGT	Heavy Duty Gas Turbine
HTH	High Temperature Heat
LTH	Low Temperature Heat
m	Mass Flow
MGT	Micro Gas Turbine
p	Pressure
PES	Primary Energy Source
PT	Power Turbine
S	Entropy
SH	Shaft
SWCD	SeaWater ©CryoDesalination
T	Temperature
TIT	Turbine Inlet Temperature
W	Work
WF	Working Fluid

Special characters

β	Pressure Ratio
ε	Ratio
η	Efficiency
k	Constant
μ , φ	Working Fluid Mass Fraction
ξ	Temperature Spread Factor
τ	Temperature Ratio
λ	Ratio
γ	Weight
χ	Ratio
Δ	Difference
R	Gas Constant
ω	Separated Water Mass Flow
θ	Ratio

Subscripts

C	Cooling effect
C	Compression
DP	Dew Point
E	Expansion
ex	Exhaust
H	High
i	Isothermal
L	Low
m	Minimum, Mechanical
M	Maximum
r	Reference
T	Temperature

INTRODUCTION

The quality of human life is strongly influenced by the availability of electricity, cold and water. Power is used in industrial and domestic (washing machine, dishwasher, etc.) contexts and for naval and ground propulsion to replace people and animals in performing heavy and difficult tasks. Cold power is characterized by the temperature at which it is available. It is used for food conservation, air conditioning, cryopreservation of living materials and cryomedical, surgical and cryobiological applications as well as industrial cryoprocesses. Pure water for drinking, domestic tasks and agricultural and industrial uses is a product increasingly in demand, especially in regions where water availability is poor. This is relevant in coastal areas: the Mediterranean, the Arabian Peninsula and the Middle East, etc. Innovative solutions for power, cold and water concurrent production are explored in studies to achieve greater environmental sustainability and economic profitability as well as high levels of reliability, availability and Easy & Cheap Maintenance (E&CM).

Traditionally, the production of these three resources is accomplished by the use of various types of machinery and apparatuses interacting together as shown in figure 1. The engine section receives a Primary Energy Source (PES) to be converted into electricity work. Heat can be bled from the engine to produce cold (e.g. by absorption system) and pure desalinated water by multiple-effect and multiflash plants.

Cold can also be produced via electrical power through vapour-compression refrigeration plants. Pure water can also be produced via electrical work by means of thermocompression desalination plants.

All the cooling is based on additional refrigeration plants connected with the engine. All the pure water is produced by plants based on evaporation and condensation processes connected with the engine.

Of course, the PES feeding the engine may be fossil-based or renewable energy sources such as biomass or solar energy, which can also be arranged in hybrid heat feed-in systems.

The paper deals with innovative and economically viable (low initial cost and reduced maintenance) solutions for concurrent production of power, cold and heat in the same ©GICE turbomachinery-based engine and production of pure water by means of novel ©CryoDesalination techniques. The paper addresses the integration between ©GICE engine layout and novel ©CryoDesalination technology. The possibility of generating multiple types of power (electric, cold & heat) in the same ©GICE engine is an innovative solution to be explored in comparison with traditional ones. The ©CryoDesalination process is based on the phenomena of water freezing and melting instead of the traditional water desalination processes based on evaporation, which involves high costs, complexity and related maintenance issues.

Various Gas Turbomachinery technologies can be employed to set up ©GICE engines for power lower than 100kW. Combustion Engine Turbocharger Technology (CETT) being produced in millions of units per year leads to cheap, reliable, compact, simple and incomparable solutions which, arranged in complex cycles (such as ©GICE) show high utilisation levels of the High Temperature Heat (HTH) fed into the cycle.

Complex arrangements based on Heavy Duty Gas Turbine Technology (HDGTT) or Aero-Derivative Gas Turbine Technology (ADGTT) can also be realized if a lot of MW is required. Moreover, looking at all the resources to be generated, the paper explores solutions for lowering PES consumption and capital costs as compared to the traditional polygeneration power plant.

The paper deals with distributed production of electricity, cold and pure water for isolated farms, small villages and industrial sites.

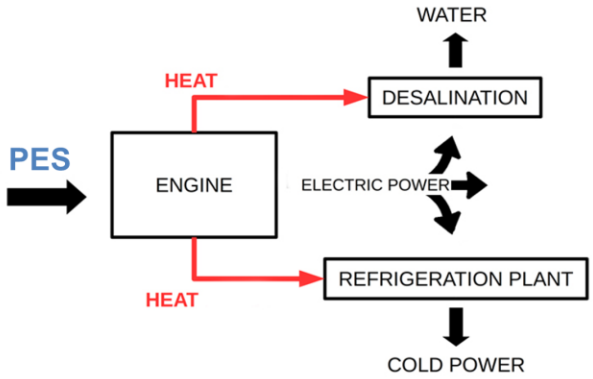

Figure 1: Traditional Polygeneration Block Scheme for the Production of Power, Cooling and Desalinated Water

Accordingly, the paper analyses the concept of an ideal ©GICE cycle to be used as a reference in such applications. The concept of High Temperature Heat (HTH) introduced into the engine is used to evaluate the cycle performance. Such a concept is then investigated in terms of feasibility taking the available CETT present in the mass flow range of the above applications.

Two case studies are presented:

1) The first one concerns 5kW power production and cooling;
2) The second one refers to a 50kW power ©GICE engine connected with a ©CryoDesalination plant. The final products being analysed are power, pure water and cold.

TECHNICAL BACKGROUND

Gas turbomachinery-based engines often called Gas Turbines (GT) are mainly connected with the Brayton cycle. The specific work of such engines increases with maximum temperature (*TIT*) and with pressure ratio (β) when it is lower than that corresponding to the maximum

work. Utilization rate of High Temperature Heat (*HTH)* is also connected with the *TIT* and β. In some circumstances, HTH coincides with thermodynamic efficiency η_{th}. Two classes of cycles have to be taken into consideration:

- Those with the exhaust temperature T_{ex} lower than that at the compressor exit T_{co}. In this case, the exhaust heat can be recovered and used for various purposes: e.g. for power production by a bottomed cycle; for heating and cooling using heat recovery systems and adequate refrigeration plants (e.g. absorption systems);
- Those with T_{ex} higher than T_{co}. In this case, a fraction of the exhaust heat can be transferred (recovered) to the working fluid (compressed air), increasing the temperature at inlet of the High Temperature Heating Device (HTHD) (T_{hi}).

Ideal Cycle

Type 2 typical Ideal cycle is the Ericsson cycle (figure 2), whose efficiency is equal to Carnot cycle efficiency. Working fluid is ideal dry air and isothermal compression work (W_{ci}) can be expressed non-dimensionally (W_{ci}) taking reference specific heat c_{pr} and reference temperature T_r into account. In this paper, $T_r = T_{c1}$ and $c_{pr} = c_{p1}$. The non-dimensional work required to perform the ideal isothermal compression is:

$$W_{CT} = \frac{W_{CT}}{c_{p1}T_{c1}} = \varepsilon \cdot \ln \beta \qquad (1)$$

where $\varepsilon = R/c_p = (k\text{-}1)/k$ is the ratio between the gas constant (R) and the constant pressure specific heat (c_p) and k is the ratio between the constant pressure (c_p) and constant volume (c_v) specific heats.
W_{CT} is equal to the Heat Rejected by the Cycle (*HRC*).
The non-dimensional isothermal expansion work is:

$$W_{ET} = \frac{W_{ET}}{c_{p1}T_{c1}} = \tau \cdot \varepsilon \cdot \ln \beta \qquad (2)$$

which is equal to the High Temperature Heat (HTH) injected into the cycle. τ is the ratio between the expansion and the compression temperatures

$$\tau = \frac{T_{e3}}{T_{c1}} \qquad (3)$$

The following relationship exists between compression work and expansion work

$$W_{ET} = \tau \cdot W_{CT} \qquad (4)$$

and it implies that the specific cycle non-dimensional work is:

$$W_T = \varepsilon \cdot (\tau - 1) \ln \beta \qquad (5)$$

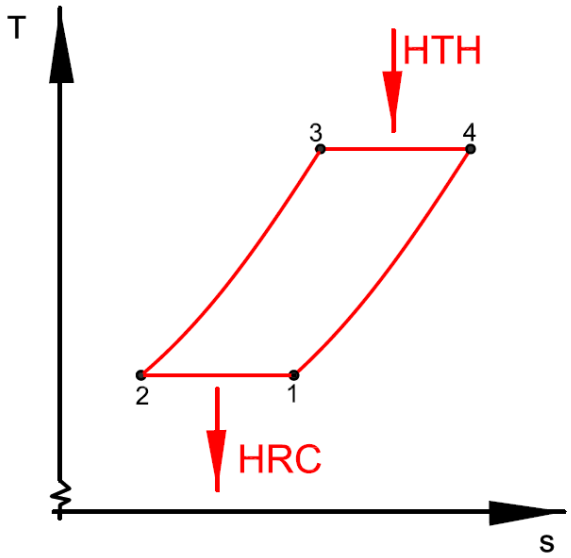

Figure 2: T-S Chart of Ideal Ericsson Cycle

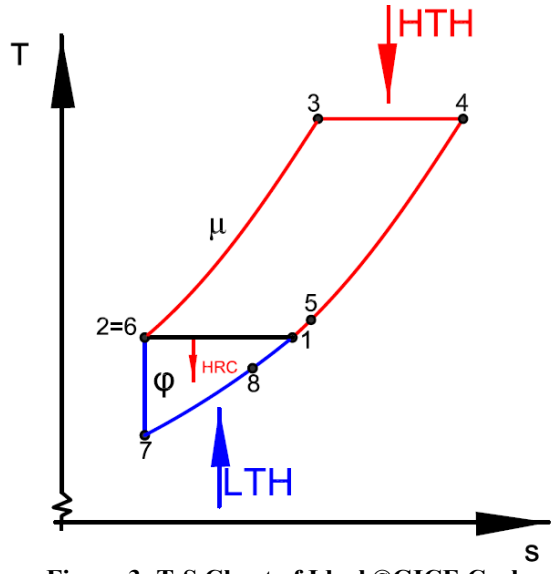

Figure 3: T-S Chart of Ideal ©GICE Cycle

The cycle efficiency is:

$$\eta_T = \frac{W_T}{W_{ET}} = 1 - \frac{1}{\tau} \qquad (6)$$

The Cycle Recovered non-dimensional Heat (*CRH*) is:

$$CRH = \tau - 1 \qquad (7)$$

The Ideal ©GICE cycle concept (figure 3) is based on the equilibrium between the high temperature expansion work

being produced by a fraction μ of the working fluid exiting the compressor and the compression work. Such a relationship is:

$$W_{CT} - \mu \cdot W_{ET} = 0 \quad (8)$$

Taking equations (1) and (2) into consideration, the fraction of the mass flow operating into the high temperature cycle section is:

$$\mu = \frac{1}{\tau} \quad (9)$$

Then, the working fluid fraction

$$\varphi = 1 - \mu = (\tau - 1)/\tau \quad (10)$$

is adiabatically expanded from the pressure $p_2 = \beta \cdot p_1$ to the ambient pressure p_1 according to the cycle scheme in figure 3.
The work delivered by this expansion is:

$$W_{PS} = \varphi \cdot \left(1 - \frac{1}{\beta^{\varepsilon}}\right) \quad (11)$$

and corresponds to the heat injected into the cycle at low temperature

$$LTH = W_{PS} \quad (12)$$

The minimum cycle temperature T_7 is:

$$T_7 = T_1 / \beta^{\varepsilon} \quad (13)$$

LTH is the heat absorbed at temperatures below the ambient T_1 along the isobaric (p_1) process, from point 7 to point 1. Ideally, *LTH* can be seen as the maximum cold power obtainable by the cycle. If a cold enclosure temperature is established lower than the compressor inlet temperature i.e. $T_8 < T_1$, the amount of the cold power (*CPs*) expressed as a non-dimensional quantity is:

$$CP_S = \varphi \cdot \left(\frac{T_8}{T_1} - \frac{1}{\beta^{\varepsilon}}\right) \quad (14)$$

The non-dimensional heat power recovered in the high temperature processes is:

$$CRH = \mu \cdot (\tau - 1) = (\tau - 1)/\tau \quad (15)$$

The ©GICE cycle high temperature heat utilization rate (efficacy) to produce useful quantities (power and cold) can be expressed as:

$$E = \frac{W_{PS} + \gamma \cdot CP_S}{HTH} \quad (16)$$

It is a coefficient for the appreciation of mechanical power and cold power.

$\gamma=0$ leads to $E_0 = \frac{W_{PS}}{HTH}$ i.e. only the power is appreciated, where E_0 represents the utilization rate of high temperature heat. $\gamma=1$ means that both power and cold are considered equally important. $\gamma = 1/COP$ represents the mechanical power consumption for cold production that is avoided when such a cold power is produced by a dedicated vapour compression refrigeration plant fed by the engine. In case of multiple production (goods *G)*, the *E* index is taken into consideration and can be expressed as:

$$E = E_0 + \frac{\sum_j \gamma_j \cdot G_j}{HTH} \quad (17)$$

where γ_j is the weight assigned to each product.

Real Working Fluid

The introduction of a real working fluid such as humid air requires a special dedicated physical model that takes phase changes such as gas to liquid and sublimation and mass separation into consideration. The species (components) variations along the processes have also been considered. In the present paper, humid air has been modelled as a mixture of O_2, N_2, CO_2, *Ar* and H_2O, each with its own thermodynamic properties. In figure 4, typical temperature pressure and enthalpy temperature charts are shown and in table 1, some of the working fluid properties are given. According to the working fluid reality, during the isothermal compression process, the Dew Point can be reached. This happens when the working fluid pressure increases p_{WF} and becomes higher than the pressure corresponding to the saturation point at dew point pressure p_{DP} and temperature T_{DP}. Under these conditions, the water vapour becomes liquid and separates from the gaseous fraction.
This process modifies the compression work and introduces some entropy production owing to equilibrium violation. Adopting as reference 1kg of compressed air at point 2, since the water vapour content corresponds to that of the water vapour saturated air at pressure p_2 and temperature T_2, the mass flow that enters the compressor for any kg that exits is:

$$m_{ci} = 1 + w_{H_2O} \quad (18)$$

As a consequence of water vapour separation, a compression working fluid reality factor λ_C can be established and then the isothermal compression real fluid work W_{CTW} is:

$$W_{CTW} = W_{CT} \cdot \lambda_C \quad (19)$$

Table 1: Triple and Critical Points for O2, N2, CO2, Ar and H2O

	Triple Point			Critical Point		
	T[K]	t[°C]	p[kPa]	T[K]	t[°C]	p[kPa]
O_2	56	-217	0	155	-119	505
N_2	63	-210	13	126	-147	339
CO_2	217	-57	517	304	31	738
Ar	84	-189	69	89	-184	490
H_2O	273	0	1	647	374	2206

Concerning the isothermal expansion process, an expansion working fluid reality factor λ_E is introduced. Accordingly, the W_{ETF} is expressed by the following equation:

$$W_{ETW} = W_{ET} \cdot \lambda_E \tag{20}$$

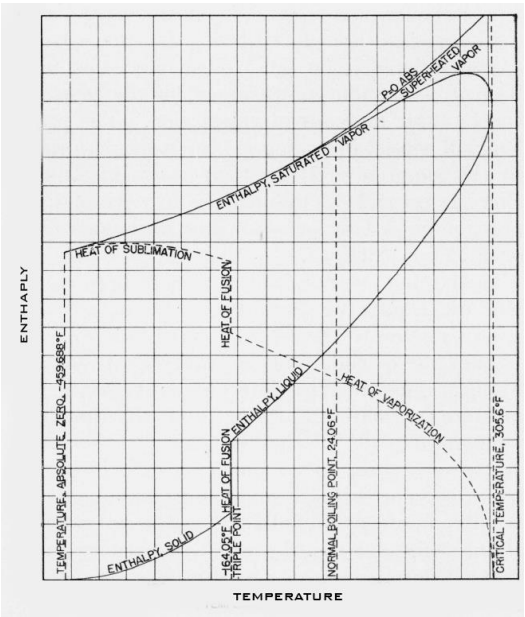

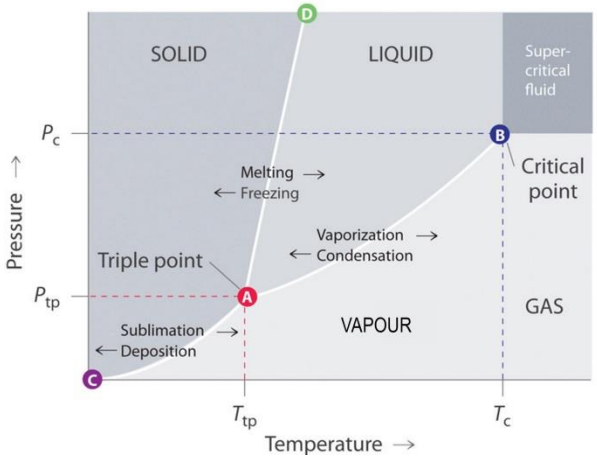

Figure 4: Pressure vs Temperature Phase Chart of a General Component [32, 33]

The λ_E reality factor takes the possibility of the internal combustion process and of the external heating process into account. In the first case, the λ_E becomes greater than one because of the additional fuel mass flow rate that contributes in the expansion work and because of the changes in the thermodynamic properties of the burning products (R changes owing to conservation of species rule). In the second case, when the WF is heated by external heating, the mass flow is unchanged, as is the composition, and the factor is equal to one.
Equation (8) is now replaced by:

$$W_{CTW} = \mu_W \cdot W_{ETW} \tag{21}$$

where φ_W is the mass flow that expands in the power turbine, equal to $1-\mu_W$. Thus, the power is still expressed as:

$$CP_{SW} = \varphi_W \cdot \frac{C_{P27}}{C_{P1}} \left(\frac{T_8}{T_1} - \frac{1}{\beta^{\varepsilon_{27}}} \right) \tag{22}$$

where c_{p27} and ε_{27} are the averaged working fluid proprieties between points 2 and 7 in figure 3.
During cold expansion, each component condensation and sublimation phenomena can occur owing to temperature and pressure reduction. This aspect has been modelled. It has been observed that according to table 1, values of O_2, N_2, CO_2 *and* Ar are far beyond such above phenomena. Only H_2O vapour mass can separate from the main stream as liquid or ice crystals depending on thermodynamic conditions. Anyway, it has been shown that the influence of such aspects is negligible.

Real Turbomachinery Processes
Isothermal compression and expansion are usually approximated by processes of Intercooled Compression (IC) and by Reheated Expansion (RE).
The IC process is accomplished by a series of phases, each carried out by a compressor and an intercooler. The compressor thermodynamic transformation phase is represented in figure 5.
The pressure levels at the intercooler inlets are:

$$p_{2Cj} = \beta_{Cj} \cdot p_{1Cj} \qquad \forall j = 1,...N_j \tag{23}$$

and at the intercooler exits are:

$$p_{3Cj} = p_{1Cj+1} = p_{2Cj} \cdot (1 - kp_{Cj}) \tag{24}$$

where $kp_{Cj} = \Delta p_{Cj} / p_{2Cj}$ is the pressure drop coefficient.

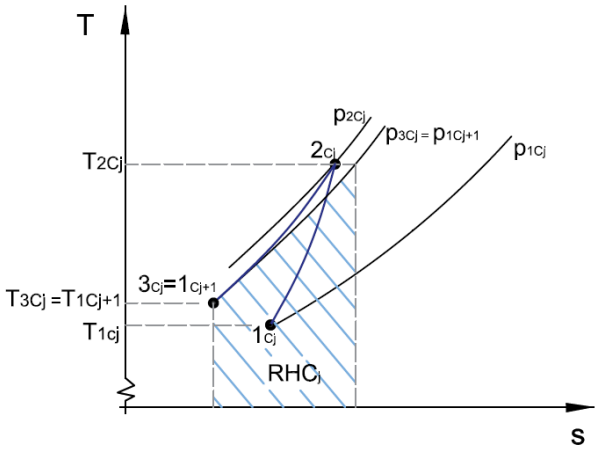

Figure 5: IC T-S Chart Scheme

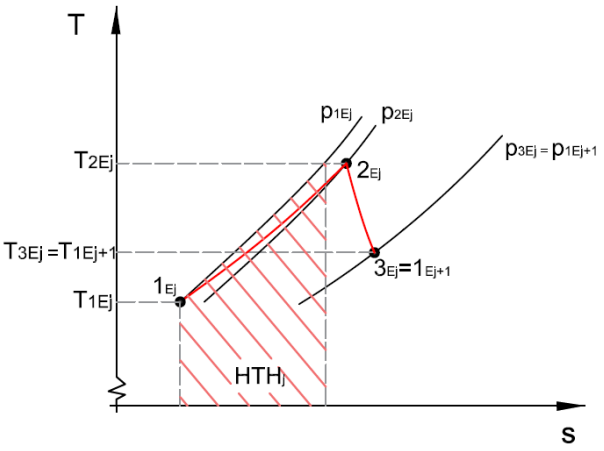

Figure 6: RE T-S Chart Scheme

The phase pressure ratio is:

$$\frac{p_{3Cj}}{p_{1Cj}} = \beta_{ICj} = \beta_{Cj}(1 - kp_{Cj}) \tag{25}$$

Of course, in thermodynamic cycles, the N_j (last) intercooler does not exist ($kp_{CNj} = 0$). Thus, the overall IC pressure ratio is:

$$\beta_{IC} = \prod_j \beta_{ICj} \tag{26}$$

The single phase work is expressed as:

$$W_{IC} = m_{Cj} \cdot \frac{\gamma_{Cj} \cdot \theta_{Cj} \cdot (\beta_{Cj}^{\varepsilon_j} - 1)}{\eta_{Cj}} \tag{27}$$

where η_{Cj} is the isentropic efficiency of the j^{-th} compressor. It depends on the corrected mass flow:

$$\mu_{Cj} = \frac{m_{Cj}\sqrt{R_{Cj}T_{Cj}}}{p_{Cj}} \tag{28}$$

and on the compressor pressure ratio.
The overall IC work is:

$$W_{IC} = \sum_j W_{ICj} \tag{29}$$

R_j changes with the composition which in turn is modified by the water vapour separation due to the liquefaction that occurs in the intercooler according to the temperature when the dew point is reached. c_{pj} is also influenced by the temperature and by the WF composition change.

$$\gamma_{Cj} = \frac{c_{pCj}}{c_p} \tag{30}$$

where γ_{Cj} is the ratio between the average constant pressure specific heat and the reference value and

$$\theta_{Cj} = \frac{T_{C1j}}{T_{1R}} \tag{31}$$

where θ_{Cj} is the ratio between the phase inlet temperature and the reference value.
When reheated expansion is also used, the composition of the working fluid changes with the internal combustion process. In the case of external combustion or solar heating, no changes in the working fluid have to be taken into consideration.
Since the single expansion shaft work is:

$$W_{Ej} = m_{Ej} \cdot \eta_{Ej} \cdot \gamma_{Ej} \cdot \tau_{Ej} \cdot \left(1 - \frac{1}{\beta_{Ej}^{\varepsilon j}}\right) \tag{32}$$

where η_{Ej} is the isentropic efficiency which depends on the expander corrected mass flow and on the expander pressure ratio.
The following relationship is for the shaft connecting the expander and the compressor

$$W_{Cj} = W_{Ej} \cdot \eta_{mj} \tag{33}$$

where η_{mj} is the mechanical efficiency of the group.
The reheated expansion phase scheme with the adopted nomenclature is shown in figure 6. According to such an *RE* scheme, the expander pressure ratio is:

$$\beta_{Ej} = \frac{p_{2Ej}}{p_{3Ej}} \tag{34}$$

where p_{2Ej} and p_{3Ej} are the pressure levels at the entrance and the exit of the expander.
The pressure at the heater (combustor) inlet is:

$$p_{1Ej} = p_{2Ej} \cdot (1 + kp_{Ej}) \tag{35}$$

That means:

$$\beta_{REj} = \beta_{Ej} \cdot (1 + kp_{Ej}) \tag{36}$$

Taking into consideration the working fluid pressure losses in the recuperator cold side,

$$p_{1Ej} = p_2 \cdot (1 - kp_{RC}) \tag{37}$$

and the hot side

$$p_{3ENj} = p_1 \cdot (1 + kp_{RH}) \tag{38}$$

the overall *IC* pressure ratio must be equal to the overall *RE* expansion pressure ratio, including pressure drops across the recuperator, and is expressed as:

$$\beta_{IC} = \frac{1 + kp_{RH}}{1 - kp_{RC}} \cdot \prod \beta_{REj} \tag{39}$$

Cycle Recuperated Heat, expressed in a non-dimensional form, taking into account the recuperator's effectiveness (ε_{REC}), minimum heat capacity and maximum temperature difference across the device.

$$H_{CRH} = \mu_W \cdot m_2 \cdot \varepsilon_{REC} \cdot \gamma_R \cdot \left(\frac{T_4}{T_1} - \frac{T_2}{T_1} \right) \tag{40}$$

where γ_R is the ratio between the average constant pressure specific heat and the reference value, m_2 is the IC compression outlet mass flow and μ_W is the fraction of the m_2 directed into the high temperature cycle. Taking the energy conservation equation into account, the outlet temperature on the cold side T_3' is:

$$T_3' = T_2 + \frac{H_{CRH}}{m_2 \cdot \gamma_R} \tag{41}$$

and on the hot side T_5 *is:*

$$T_5 = T_4 - \frac{H_{CRH}}{m_4 \cdot \gamma_{45}} \tag{42}$$

where m_4 is the reheated expansion outlet mass flow and γ_{45} is the ratio between the average constant pressure specific heat between T_4 and T_5. According to the above, the heat received by the heater (combustor) is:

$$HTH_j = \gamma_{hj} \cdot \left(\tau_j - \frac{T_{1Ej}}{T_1} \right) \tag{43}$$

where τ_j is the ratio between the expander inlet temperature and the reference value. Thus:

$$HTH = \sum_{j=1}^{Nj} HTH_j \tag{44}$$

HTH being the High Temperature Heat entering into the cycle.

Adopting an adequate Turbomachinery Technology Data Base that allows the selection of the compressor and expander wheel sizes as well as the heat transfer device sizes, it is possible to arrange a ©GICE engine for best performance.

©CryoDesalination

CryoDesalination is a novel technique for the production of pure water without the expensive and labour-intensive use of centrifuges, filters and various other separation equipment that require a great deal of maintenance and frequent plant shut-downs. This undesired aspect can be avoided by use of a flotation medium. The CryoDesalination process is based on a phenomenon found in nature:

- When salt water freezes the resulting ice is pure
- When melted, such ice becomes fresh water

Previous attempts at freeze desalination were not commercially viable because the pure ice could not be separated effectively from the surrounding brine.

CryoDesalination uses flotation to solve this "ice-brine separation problem". Ice and brine have different specific gravities. By introducing Cryosol (a non-toxic fluid that is immiscible with water and has a specific gravity between that of ice and that of brine) into the process, the mixture can be separated by flotation and pure water can be harvested. The ice is kept as a slurry, which permits pumping, direct contact heat transfer, and energy recovery. According to the above, figure 7 shows the flow chart for the ©CryoDesalination processes. The following CryoDesalination Process Flow Chart applies to seawater desalination as well as to all freeze salinity conditions encountered in other industrial applications. The only differences between cases would be the operating pressures and temperatures; they are a function of the salinity of the reject brine.

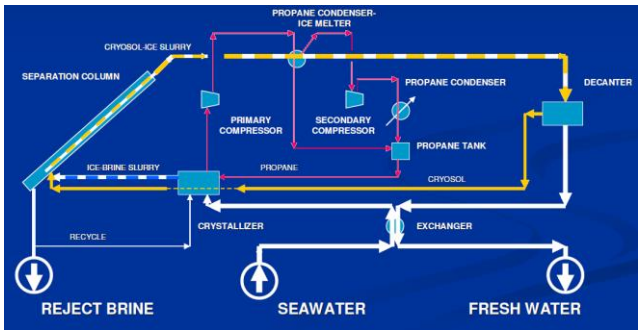

Figure 7: ©CryoDesalination Schematic Process Flow

The white lines represent the flow of water. The yellow lines represent Cryosol, the non-toxic flotation medium. The dashed lines represent ice slurried in either water or Cryosol. The red lines show the refrigerant propane loop.
Seawater cooled by the outgoing fresh water stream enters the Crystallizer where it is mixed with liquid propane. As the propane comes in contact with the incoming seawater in the Crystallizer, it vaporizes and ice is formed. The propane vapours are compressed, condensed, and recycled to the Crystallizer.
Ice and brine exit the Crystallizer as a slurry. Cryosol is added to the slurry stream. The combined stream enters the Separation Column. Due to differences in density, the Cryosol separates the ice and brine. The brine flows out the bottom of the column, and then on to disposal. Ice and Cryosol leave the column top and flow through the Propane Condenser/Ice Melter wherein the ice melts while carried by Cryosol. It moves on to the Decanter, where the stream separates easily into two layers because Cryosol is immiscible with water. The Cryosol layer is recycled to the process. The water layer is withdrawn as the desired Fresh *Water Product.* Plants based on ©GICE engines coupled with CryoDesalination present many advantages: they are simpler, more efficient, and less expensive to build and operate than thermal or reverse osmosis desalination processes. They require no costly membrane elements, no exotic metals and no chemicals. They are considerably more environmentally friendly.

CASE STUDIES

Two different case studies are presented in the next sections of the paper. CASE A shows the application of the ©GICE engine for the concurrent production of power and cold. This case is named 2SHPT because the engine is made of two freestanding spools (2SH) for compressed air generation and of one cold Power Turbine (PT) for power production and cooling. 5kW Net power has been assumed for CASE A. The other case study, CASE B, named 3SHPT&SWCD, presents a ©GICE engine layout consisting of three freestanding spools and 1PT, whose exhaust is integrated within the Seawater ©CryoDesalination (SWCD) plant. In CASE B, the size of the plant is calculated for a 1kg/s mass flow rate at the inlet of the compression process. Ambient temperature *T1=25°C,* pressure *p1=101.3kPa* and 40% Relative Humidity have been assumed.

Case A – 2SHPT

In exploring the ©GICE concept, the RO3 Turbomachinery DB was considered for establishing compressor and expander sizes and efficiencies. The 2SHPT arrangement is shown in figure 8. Compression is carried out by means of two compression phases whose intercooler stream exits at a temperature 10°C higher than T_1. Two reheated expansion phases drive the related compressor, and performance is influenced by the number of shafts and by the turbine inlet temperature.

The Roma Tre Turbomachinery Database and the search for the best HTH utilization, taking into consideration power production and cooling, (cold enclosure temperature being assumed to be 0°C), informed engine performance, architectures and sizes.
Calculations have been performed for overall compression pressure ratios between 3 and 8. A maximum temperature of 900°C and regeneration degree of 0.9 have been assumed. Results have been presented in figure 9 for 5kW of net generated power. It should be pointed out that an increase in the pressure ratio leads to a significant reduction in the cold *PT* exhaust temperature (violet line on the chart). At the same time, when the pressure ratio increases, the working fluid mass flow decreases because of the given power. In addition, the heat power transferred in the recuperator decreases, leading to smaller heat transfer surface and weights (cost).
Performance E and E_0 decrease when the overall pressure ratio increases. The results of the calculations concerning the turbomachinery sizes and architecture show that the exducer diameters of the 1st and the 2nd compressor are $D_{C1}=69mm$ and $D_{C2}=58mm$, respectively. The inducer diameters of the corresponding driving expanders are $D_{E1}=84mm$ and $D_{E2}=72mm$.
The shaft speeds of the two freestanding groups are *n1=95krpm* and *n2=105krpm*. The power turbine wheel has been also established. The cold expansion takes place in a single power turbine where $D_{PT}=64mm$.
Accordingly, the choice of ©GICE engine operating parameters such as pressure ratio and maximum operating temperature depend on cost compromise.

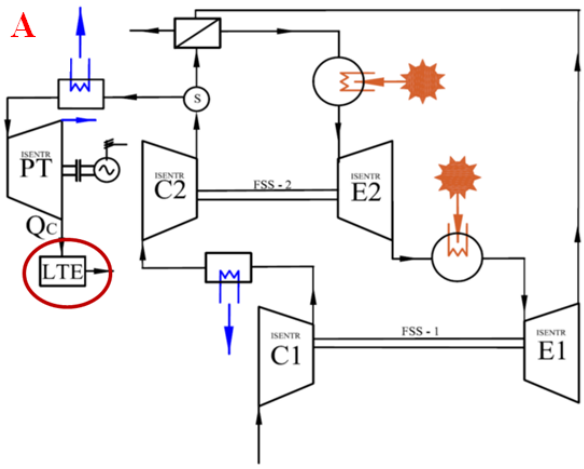

Figure 8: ©GICE Engine – 2SHPT

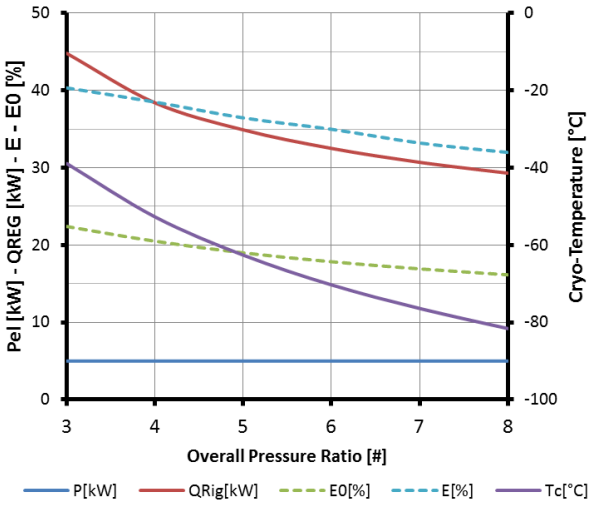

Figure 9: ©GICE 2SHPT Arrangement for Electric Power of 5kWe

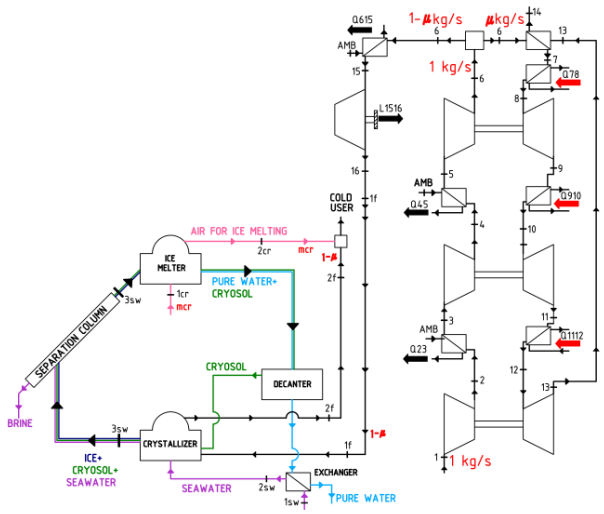

Figure 10: 3SHPT&SWCD – CASEB#1 Cold Power Used only for SWCD

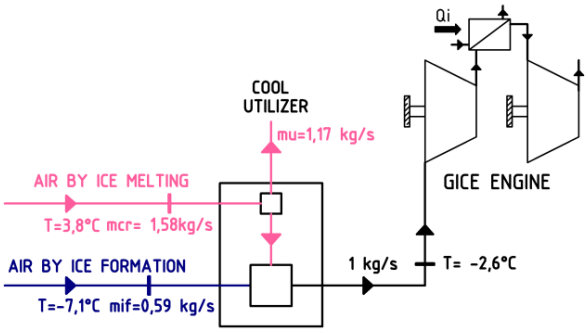

Figure 11: 3SHPT&SWCD – CASEB#2 Cold Power Used for Internal Heat Recovery & SWCD

Case B – 3SHPT&SWCD

The integration of ©GICE engines with ©CryoDesalination concurrently produces power and pure desalinated water and cold to approximately 0°C. The available very low cryogenic temperature stream at the ©GICE cold expander exit can be used for industrial purposes and for seawater cryogenic desalination. At the very end, three products result concurrently: power, pure desalinated water and cold power (available at approximately 0°C) which could be used for various purposes, including air conditioning.

For Case B, two possibilities have been explored for low temperature cold power utilization. In the first, the entire amount of cold power is directed to the ©CryoDesalination Plant (CaseB#1); the second introduces the possibility of internally recovering the cold power to lower the air temperature at the compressor inlet. Engine performance increases (CaseB#2).

The engine arrangement is the same for the two sub-cases. It is made of three freestanding spools (3SH) and one cold power turbine (PT), whose exhaust temperature is lower than that of the 1st compressor inlet. After the three compression phases, the overall inlet mass flow is split into two sub-streams. The first one is processed into the clockwise (direct) cycle flowing through three reheated expansion phases. The second one flows into an intercooler and then expands in the cold power turbine, until the ambient p_1 reaches an exhaust cryo-temperature. The air cryo-temperature stream is used for the seawater desalination process, as a substitute for the cryo-pentane stream.

Diagram of such cases: CaseB#1 and CaseB#2 are presented in figures 10 and 11, respectively. Taking results of Case A into consideration, performance is also influenced by engine operating parameters and boundary conditions for such a 3SHPT&SWCD.

Efficiencies of compressors and expanders have been selected according to the technology levels, corrected mass flows and pressure ratios. Calculations have been carried out for a given inlet compressor mass flow of 1kg/s. Performances (e.g. generated power, exhaust cryo-temperature, desalinated seawater mass flow, etc.) have been calculated assuming three freestanding spools, 25°C inlet temperature, 101.3kPa inlet pressure and 40% relative humidity. Feasibility of various options has been investigated.

Compressor and expander efficiencies have been set according to the technology DB. Maximum engine operating temperature to ensure safe and stable operating conditions has been assumed as T_{MX} = 900°C. CaseB#1 results are reported in figure 12. Engine performance together with the desalination plant outcomes are reported as compared with the overall compression ratio. The green dotted line is the exhaust cryo-temperature. Increasing the overall pressure ratio, cryo-temperature decreases. Power, cold power and pure desalinated water increase.

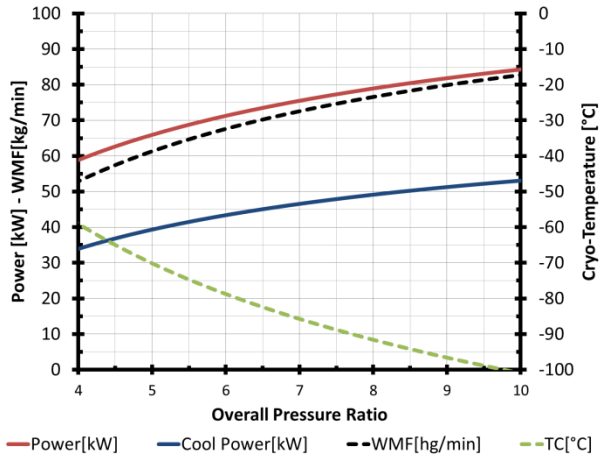

Figure 12: 3SHPT&SWCDLayout Performance Analyses VS Overall Pressure Ratio

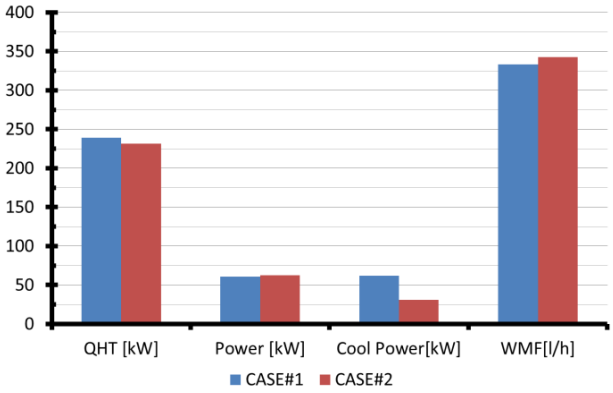

Figure 13: 3SHPT&SWCD CaseB#1 and CaseB#2 Comparison

Under these conditions, the *HT* cycle is performed by μ*=421g/s* of working fluid, while φ*=579g/s* flows through the cold cycle. Assuming 0°C as reference for the cold enclosure, all the cold power is used by the ©CryoDesalination Process. Taking into account the compressor inlet arrangement depicted in figure 11 to improve the above performance, the WF temperature at the compressor inlet is reduced to -2°C.

A comparison between the performance of these plant layouts is presented in figure 13. Calculations have been carried out for an overall pressure ratio of 5.4.

WF is split into a μ*=406 g/s* portion for the High Temperature Cycle for air compression and a φ*= 594 g/s* portion that flows through the cold power turbine, generating power and cooling.

Results show that HTH utilization is higher in CaseB#2 (red columns) and that a larger amount of water can be obtained. Power is almost unaffected by the flow treatment at the compressor inlet, while cold power availability becomes less than one-half, making the layout less effective for cryogenic purposes.

CONCLUDING REMARKS

The paper has demonstrated the possibility of arranging ©GICE Micro Gas Turbines producing power and cryo-temperature stream without additional refrigeration machinery such as vapour compression plants and absorption systems. The engine arrangement may be fed by solar energy using a suitable receiver capable of dumping the sun's high-frequency DNI fluctuations (up to 30-45min absence of sun). Hybridization of the engine receiver can be taken into consideration by external combustion and heat recovery of the furnace exhaust heat.

The utilization rate of the HTH assumes interesting values, over 40% when power and cold are the production requirements. Integration with the ©CryoDesalination plant leads to concurrent generation of power, pure water and cold at around 0°C to be used for air conditioning or other purposes. Increasing the turbine inlet temperature, the mass portion expanding in the cold turbine increases, leading to better performance and to a reduction of costs.

ACKNOWLEDGEMENTS

The Authors acknowledge the EU and Roma Tre University for their support under the 'Optimized Microturbine Solar Power System' OMSoP project.

BIBLIOGRAPHY

[1] Janajreh I.; Water Desalination via Direct Contact Membrane Distillation, *Energy and Water in the Gulf Cooperation Council Countries EWGCC 2016*, 12-14 April 2016, Ras Al Khaimah, UAE

[2] Safarik M.; Alternative Approaches to Water Desalination Without Chemicals — the MED and MVC— MED Processes, *Energy and Water in the Gulf Cooperation Council Countries EWGCC 2016*, 12-14 April 2016, Ras Al Khaimah, UAE

[3] Moser Massimo.; Assessment of Utility – Scale Solar Desalination, *Energy and Water in the Gulf Cooperation Council Countries EWGCC 2016*, 12-14 April 2016, Ras Al Khaimah, UAE.

[4] Tian Y., Zhao C.Y.; A review of solar collectors and thermal energy storage in solar thermal applications, *Applied Energy 104 (2013) 538-553, Elsevier.*

[5] Yilanci A., Dincer I., Ozturk H.K.; A review on solar-hydrogen/fuel cell hybrid energy systems for stationary applications, *Progress in Energy and Combustion Science 35 (2009) 231-244, Elsevier.*

[6] Kuravi S., Trahan J., Yogi Goswami D., Rahman M. M., Stefanakos E. K.; Thermal energy storage technologies and systems for concentrating solar power plants, *Progress in Energy and Combustion Science 39 (2013) 285-319, Elsevier.*

[7] Kane M., Larrain D., Favrat D., Allani Y., Small hybrid solar power system. *Energy 28 (2003) 1427-1443, Elsevier.*

[8] Zalba B., Marin Josè M., Cabeza L.F., Mehling H., Review on thermal energy storage with phase change:

materials, heat transfer analysis and applications, *Applied Thermal Energy 23 (2013) 251-283, Elsevier.*

[9] Zini G., Tartarini P.; Hybrid Systems for solar hydrogen: A selection of case-studies, *Applied Thermal Energy 29 (2009) 2585-2595, Elsevier.*

[10] Houcine I., BenAmara M., Guizani A., Maalej M.; Pilot plant testing of a new solar desalination process by a multiple-effect-humidification technique, *Desalination 196 (2006) 105-124, Elsevier.*

[11] Hou S.; Two-stage solar multi-effect humidification dehumidification desalination process plotted from pinch analysis, *Desalination 222 (2008) 572-578, Elsevier.*

[12] Sagie D., Feinerman E., Aharoni E.; Potential of solar desalination in Israel and in its close vicinity, *Desalination 139 (2001) 21-33, Elsevier.*

[13] - Alavi B., Cerri G., Chennaoui L., Mazzoni S.: '*Power, Cool and Water Production by Innovative Cycles Fed by Solar Energy'*, SASEC 2015, May 11-13,2 015, South Africa

[14] - Alavi B., Cerri G., Chennaoui L., Giovannelli A., Mazzoni S.: *'MGT Cycles for Solar Dish Applications*', Proceedings of SEEP 2014, 23-25 November 2014, Dubai

[15] Chen J., Yan Z., Chen L., and Andresen B., Efficiency Bound of a Solar-Driven Stirling Heat Engine System, *International Journal of Energy Research*, 22,805 - 812, 1998

[16] Cerri G., Bernardini I., Giovannelli A., Chennaoui L., A Gas Turbine High Efficiency Cycle Fed by Concentrated Solar Power, The 21stISABE Conference, Busan, Korea, Sept.9-13, 2013

[17] Jonsoon M., and Yan J., Humidified Gas Turbines - A Review of Proposed and Implemented Cycles, *Energy*, 2005, Vol. 30, Issue 7, pp. 1013 - 1078

[18] Horlock J.H., Advanced Gas Turbine Cycles, *Whittle Laboratory Cambridge*, UK, 2003

[19] Cerri G., and Arsuffi G., Steam Injected Gas Turbine Integrated with a Self-Production Demineralized Water Thermal Plant, *Journal of Engineering for Gas Turbines and Power*, Vol. 110, no. 1, January 1988, pp. 8 - 16

[20] Cerri G., and Sciubba E., Aero - Derived Reheat Gas Turbine with Steam Injection into the Afterburner, *ASME Winter Annual Meeting,* Boston - USA, December 13 - 18,1987

[21] Cerri G., and Arsuffi G., Steam Injected Gas Generators in Power Plants, *ASME COGEN - TURBO International Symposium*, Montreux - Swiss, September 2 - 4, 1987

[22] Hendricks R.C., Shouse D.T., and Roquemore W.M., Water Injected Turbomachinery, *NASA/TM* 2005 - 212632

[23] Cerri G., and Arsuffi G., Calculation Procedure for Steam Injected Gas Turbine Cycles with Autonomous Distilled Water - Production, *International Gas Turbine Congress*, Dusseldorf, FRD, June 8 - 12, 1986, ASME pap. n. 86 - GT - 297

[24] Elgendy Y.A., Solar Dish-Ericsson Engine: A Novel Solar Technology for the 21st Century, *Foundation Annual Research Forum Proceedings*: Vol. 2011, EGP12

[25] Kussul E., Baidyk T., Blesa J.S., and Bruce N., Support Frame for Solar Concentrator with Flat Mirrors, Device Assembly Method and Ericsson Heat Engine, *Recent Researches in Environmental and Geological Sciences*, ISBN: 978 - 1 - 61804 - 110 – 4

[26] Mikalsen R., and Roskilly A.P., A Review of Free-Piston Engine History and Applications, *Applied Thermal Engineering*, Vol. 27, Issues 14-15, Oct. 2007, pp. 2339- 2352

[27] Kussul E., Makeyev O., Baidyk T., and Olvera O., Ericsson Heat Engine for Small Solar Power Plants, *International Conference on "Low-cost, electricity generating heat engines for rural areas*" Nottingham, April 2 - 3, 2012

[28] Bortolini M., Gamberi M., Graziani A., Pilati F., Optimization of a Gas Compression Refrigerator for Drinking Water Production Through Air Dehumidification, *13th Internal Conference on Clean Energy*, Istanbul, Turkey, June 8-12,2014

[29] Sanchez–Orgaz S., Medina A., and Calvo Hernandez A., Maximum Overall Efficiency for a Solar–Driven Gas Turbine Power Plant, *International Journal of Energy Research*, August 2012, DOI: 10.1002/er.2967

[30] Dickey B., Test Results from a Concentrated Solar Microturbine Brayton Cycle Integration, *Proceedings of ASME Turbo Expo*, Vancouver, Canada, June 6 - 10, 2011

[31] Cerri G. et Al., 'Report on Short Term Storage Testing and Evaluation', OMSoP Deliverable 1.2, Roma Tre University, Department of engineering, 2015.

[32] Cyril H. Meyers, Carl S. Cragoe, and Eugene F. Mueller, 'Table and Mollier Chart of the Thermodynamic Properties of 1, 3-Butadiene', U. S. Department of Commerce National Bureau of Standards, Research Paper RP1844 Volume 39, December 1947

[33] http://2012books.lardbucket.org/books/principles-of-general-chemistry-v1.0/s15-07-phase-diagrams.html